

# Proteus: Enhanced mmWave Leaf Wetness Detection with Cross-Modality Knowledge Transfer

Yimeng Liu, Maolin Gan, Huaili Zeng, Yidong Ren, Gen Li, Jingkai Lin, Younsuk Dong, Xiaobo Tan, Zhichao Cao  
Michigan State University, USA

## Abstract

Accurate leaf wetness detection is essential to understanding plant health and growth conditions. The mmWave radar, with its sensitivity to subtle changes, is well-suited for leaf wetness detection. Existing mmWave-based approaches utilize the Synthetic Aperture Radar (SAR) algorithm to generate image-like inputs and rely on multi-modality fusion with an RGB camera to classify leaf wetness. However, the lack of understanding of SAR-based mmWave imaging limits its accuracy in various environments. This paper presents Proteus, a novel way of understanding mmWave SAR imaging. We design a noise reduction algorithm to reduce speckle noise and improve image clarity for SAR-based mmWave imaging. Then, we incorporate phase angle data to enrich SAR texture information to capture high-resolution surface details, increasing informative features for precise wetness assessment in complex plant structures. Additionally, we introduce a cross-modality Teacher-Student network, using an RGB-based teacher model to guide the mmWave SAR-based student model for feature extraction. This network transfers the explicit knowledge in the RGB image domain to the mmWave image domain. We use commercial-off-the-shelf mmWave radar to prototype Proteus. The evaluation results show that Proteus achieves up to 96.3% accuracy across varied environmental scenarios, outperforming state-of-the-art methods.

## CCS Concepts

- Computer systems organization → Sensors and actuators;
- Applied computing → Agriculture.

---

Permission to make digital or hard copies of all or part of this work for personal or classroom use is granted without fee provided that copies are not made or distributed for profit or commercial advantage and that copies bear this notice and the full citation on the first page. Copyrights for components of this work owned by others than the author(s) must be honored. Abstracting with credit is permitted. To copy otherwise, or republish, to post on servers or to redistribute to lists, requires prior specific permission and/or a fee. Request permissions from permissions@acm.org. *SenSys '25, May 6–9, 2025, Irvine, CA, USA*

© 2025 Copyright held by the owner/author(s). Publication rights licensed to ACM.

ACM ISBN 979-8-4007-1479-5/25/05

<https://doi.org/10.1145/3715014.3722052>

## Keywords

AIoT, Wireless Sensing, RF Imaging, Knowledge Transfer

## ACM Reference Format:

Yimeng Liu, Maolin Gan, Huaili Zeng, Yidong Ren, Gen Li, Jingkai Lin, Younsuk Dong, Xiaobo Tan, Zhichao Cao. 2025. Proteus: Enhanced mmWave Leaf Wetness Detection with Cross-Modality Knowledge Transfer. In *The 23rd ACM Conference on Embedded Networked Sensor Systems (SenSys '25), May 6–9, 2025, Irvine, CA, USA*. ACM, New York, NY, USA, 15 pages. <https://doi.org/10.1145/3715014.3722052>

## 1 INTRODUCTION

The rising frequency and severity of plant disease outbreaks threaten global food security, agricultural productivity, and biodiversity [15, 53, 54, 61, 70]. These outbreaks, driven by pathogens such as fungi, bacteria, and viruses, lead to substantial yield losses and ecological damage, costing an estimated 220 billion annually [54, 61]. Precision agriculture has become essential to improve productivity while reducing environmental impact [3, 5, 16, 57]. A key component is monitoring environmental factors that foster disease. Leaf Wetness Duration (LWD), the time water remains on leaf surfaces [43, 55] is crucial for fungal and bacterial pathogens growth [28, 75]. Therefore, accurate LWD detection is vital for managing crop diseases and enabling timely interventions in crops like strawberry [30, 39], cucumber [22], and sweet cherry [65].

Researchers have introduced various modalities to improve LWD detection systems, including leaf wetness sensors (LWS) [20, 46, 67], RGB/infrared cameras [30, 76], and Terahertz [31]. However, these methods still struggle with low accuracy in various environments and complex deployment. Current state-of-the-art systems [18, 36] for leaf wetness detection primarily utilize mmWave radar imaging to build an orthogonal information channel. However, none of the existing systems have comprehensively utilized and analyzed the mmWave-based features for reliable wetness detection. mmLeaf [18] employs a Synthetic Aperture Radar (SAR)-based mmWave imaging approach [80] to obtain detailed plant images, but a lack of understanding of the SAR image feature leads to struggles in achieving high detection accuracy. Hydra [36] efficiently extracts the focus on multi-modality features combined with the RGB camera and

mmWave SAR image in diverse environments. Adonis [35] uses mmWave for leaf wetness level detection but primarily focuses on comparing different wetness levels rather than directly extracting wetness features. Three key limitations are illustrated as follows:

**Intense Noise in mmWave Radar Data** Existing SAR-based mmWave imaging inherently adds speckle noise due to the coherent nature of radar waves. The multiple scattered signals within a resolution cell interfere with each other [37], particularly in challenging environments (e.g., irregular plant 3D structure, leaf vibration, moderated wind). If speckle noise appears in the water drop areas, the signal-to-noise ratio (SNR) will be reduced. On the other hand, the speckle noise in random areas may create fake water drops. Noise will mislead the machine learning model for classification. Therefore, the accuracy will be degraded.

**Limited Wetness Feature Spaces** The existing mmWave-based leaf wetness detection model relies heavily on pixel intensity patterns in the SAR image to capture the wet leaf texture. Ideally, the water drop will reflect more signals than the dry leaf areas, producing a high pixel intensity. However, the pixel intensity of the SAR image indicates relative intensity, which is not a stable indicator of wetness. Many other factors, such as leaf surface roughness, leaf density, relative position, and leaf size, can significantly influence different plants and environments. These variations make it challenging to build a uniform feature space to consistently detect wetness in general environments, as low-dimensional pixel intensity changes may reflect surface characteristics unrelated to wetness. Thus, relying solely on pixel intensity may result in inaccurate leaf wetness identification due to variations in crops and environments.

**Constrained Feature Extraction and Explainability.** Using mmWave-based SAR imaging can produce apparent features only if non-overlapped leaves appear in a radar's field-of-view (FoV) and the radar directly faces the leaf. The reflection of water drops can be maximized, keeping a high SNR. However, physical mmWave radar deployment constraints in natural environments introduce a significant challenge with a good relative position. In addition, complex plant structures will bring multi-path noises to blur the pixel intensity. The two factors above make it difficult to obtain high SNR features from SAR images for leaf wetness detection in practice. The existing machine learning model lacks an explanation for efficiently extracting the low-SNR leaf wetness features to guarantee classification accuracy in real-world applications.

To address these limitations, this paper introduces Proteus with a novel approach to mmWave SAR image analysis by borrowing the knowledge from the RGB image domain. The method for Proteus involves a feature-enhanced mmWave

imaging system for accurate leaf wetness detection. We generate high-SNR images, construct informative and explainable features to enhance the mmWave-based image, and use a machine-based method to understand the features. To enable these, our techniques include developing a denoising method, cooperating with new texture information, and leveraging the well-trained feature space of another modality to teach mmWave imaging, known as cross-modal knowledge transfer. By doing so, Proteus improves the feature of the mmWave image and uses machine learning-based methods to understand the mmWave SAR-based imaging deep. Specifically, Proteus includes three key components:

**Speckle Noise Reduction.** We aim to reduce speckle interference while preserving critical leaf texture features in a mmWave image. We observe that the speckle noise is a granular, salt-and-pepper-like texture. The high-frequency pattern challenges the interpretation of object contours and textures. We use a computer vision-based algorithm to mitigate the speckle pixels with their surrounding pixels. The image clarity is enhanced in this way, allowing the system to focus on essential wetness-related features.

**Enhanced Image Informativeness with Phase Angle.** In addition to the intensity patterns on existing mmWave images, we adopt other orthogonal features to enhance the informativeness of the images. The phase angle indicates the angular displacement between transmitted and received signals. The water on a leaf changes the received phase angle by introducing additional phase shifts due to the altered dielectric properties [4, 9, 32]. We incorporate phase angle data into SAR imaging, which enriches the captured surface texture and reveals fine details. This enhancement provides a more comprehensive view of leaf wetness distribution, leveraging the extra information to detect minute wetness changes accurately.

**Cross-Modal Teacher-Student Network.** We aim to construct an augmented feature space that enables machine learning models to capture wet pixels accurately. Existing work [36] has shown that RGB images can capture apparent wetness features with good lighting conditions, constructing an excellent feature space for image recognition models. We aim to transfer the knowledge from the RGB-image feature space to our mmWave-image feature space. To further improve feature extraction, we adopt a cross-modality Teacher-Student network that leverages RGB images for guidance. The RGB-based teacher model is pre-trained on apparent wetness features in our setup. It guides the SAR-based student model in recognizing and learning subtle wetness patterns. Combined with depth fusion, it enables the comprehensive extraction of plant features within a 3D structure. We utilize LSTM, which efficiently captures temporal dependencies.

This cross-modality approach enhances the model's ability to detect wetness with higher accuracy and enriches its adaptability across different plants.

We implement Proteus using commercial off-the-shelf hardware components. In the evaluation, we consider various types, sizes, densities, and environments, including indoor and outdoor. The extensive evaluation of Proteus demonstrates its excellent performance in various settings. It achieves 96.3% accuracy in distinguishing leaf wetness or dryness. It achieves less than 5 minutes of error in LWD detection, which outperforms the state-of-the-art mmWave-based system by about 10.77% accuracy. In addition, with the enhanced mmWave imaging, the accuracy of the multi-modality leaf wetness detection system can be improved by about 3.97%.

The contributions can be summarized as follows:

- We resolve the challenging problem of interpreting and enhancing SAR-based mmWave images for accurate leaf wetness detection. With cross-modality knowledge transfer from an RGB camera, we significantly enhance the informativeness of the feature for leaf wetness classification.
- We develop targeted techniques to enhance mmWave images. Firstly, we designed a noise reduction method to remove speckle noises on a SAR image. Secondly, phase angle features are integrated to enhance the SAR image with rich texture details. Finally, we design an adaptive Teacher-Student framework to transfer the knowledge from the RGB to the mmWave image domain.
- The system has been prototyped and extensively tested on various plant types under diverse environmental conditions, achieving 96.3% accuracy on wetness detection and less than 5 minutes error on leaf wetness duration detection, which outperforms the state-of-the-art.

## 2 PRELIMINARY

### 2.1 Definition of Leaf Wetness

Leaf wetness duration refers to the period a leaf remains wet, which is crucial for plant disease management [55]. Accurate LWD detection depends on identifying leaf wetness, which indicates the presence of water on the leaf surface [44, 68]. Based on the ground truth detection from the state-of-the-art leaf wetness section system Hydra [36], specified in Section 4.2. We set up a calibrated moisture meter, which is used for surface moisture detection to determine leaf wetness. The meter is calibrated in a dry, ventilated environment to set a baseline threshold for dryness. If the reading exceeds this threshold, the leaf is classified as wet; otherwise, it is considered dry.

### 2.2 mmWave SAR Imaging

The mmWave refers to electromagnetic waves with wavelengths in the millimeter range, typically between 1 and 10 millimeters. This short wavelength makes the radar highly sensitive to minor surface texture changes, allowing it to detect subtle details accurately, which is essential for identifying leaf wetness. The mmWave's sensitivity to material properties makes it particularly effective for leaf wetness detection. Different materials exhibit distinct permittivity values, which impact how they reflect mmWave signals. Since water has a high permittivity compared to dry leaf surfaces, wet leaves reflect mmWave signals differently. The difference makes it possible to distinguish wet leaves from dry ones [18, 36].

SAR is a remote sensing technology that leverages the movement of the radar system to generate high-resolution images by simulating a larger antenna aperture. This technique enables mmWave radar to capture the fine details of surface structures, providing the potential to detect leaf wetness via mmWave images. We conduct mmWave SAR experiments to investigate leaf wetness detection further and observe wetness features to demonstrate several limitations. We develop a 2-axis mechanical testbed for SAR imaging and placed an RGB camera at the center of the scanning area to capture visual information. The radar signals are extracted from a stationary leaf and plant positioned 200 mm from the radar.

**Pixel Noises in SAR:** In Figure 1, we compare the imaging results of a plastic "A" target captured with a standard camera and SAR. The plastic material, chosen for its low reflectivity and rough surface texture, mimics the characteristics of a leaf surface. The camera image in Figure 1a captures the target's shape and texture with clarity, while the SAR image in Figure 1b is heavily impacted by speckle noise in the areas of shape "A". Noise arises from the scattering of coherent radar waves, which interfere constructively and

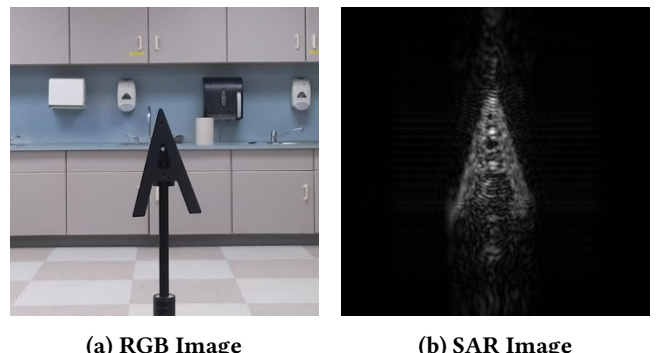
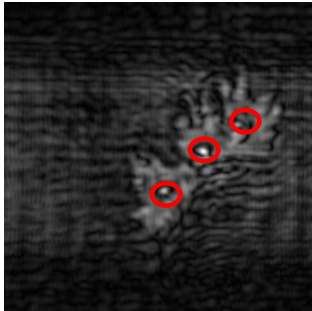


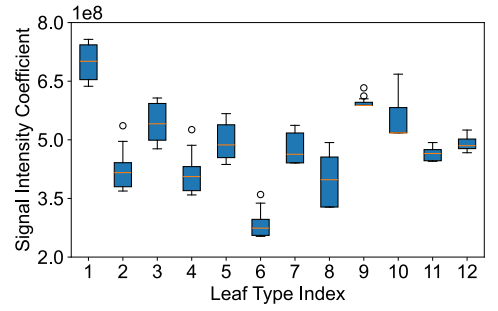
Figure 1: Speckle noise shown in SAR imaging.



(a) Leaf RGB Image

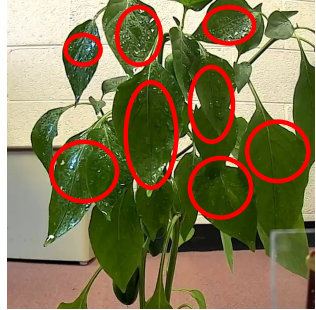


(b) Leaf SAR Image

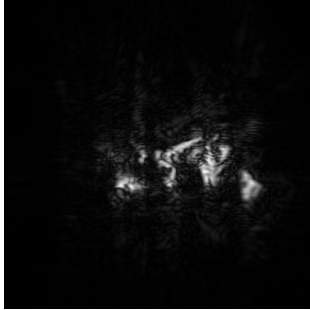


(c) Signal intensity distribution

**Figure 2: In simple leaf structures, wetness features are visually detectable in SAR imaging; however, the intensity of these features varies significantly between different types of leaves.**



(a) Plant RGB Image



(b) Plant SAR Image

**Figure 3: Limited wetness feature in complex structure.**

destructively [40, 84]. The salt-and-pepper noise makes distinguishing precise contours and extracting texture details from the image challenging. It emphasizes the need for effective noise reduction in SAR-based leaf wetness detection.

**Limitation of Pixel Intensity Features:** We conduct experiments using leaves with simple droplets and no overlapping. Figure 2a shows the RGB images, where clear droplets circled in red are easily detectable. Figure 2b displays SAR images with distinct droplet features in the corresponding areas. That indicates SAR imaging can effectively capture wetness features. However, the intensity is a relative value among all pixels. To further analyze these features, we collect 12 different types of leaves with variations in surface roughness. We generate an image for each leaf type without overlapping leaves and apply a few droplets. The experiment repeats 10 times for each leaf type. We identify the droplet areas in SAR images based on their distinct features and the corresponding droplet area of RGB images. We extract the intensity feature in the areas. The boxplot in Figure 2c shows a significant variance in intensity across different leaf types. It reveals that intensity is inconsistent, which limits the reliability of wetness features across groups.

**Blurred Image under Complex 3D Plant Structure:** We extend our experiments to analyze wetness detection on entire plants. As shown in Figure 3a, distinct water features, circled in red, are visible in the RGB images. The SAR image is captured at 210 mm from the testbed shown in Figure 3b. Compared with Figure 2b for the wetness feature in simple leaf structures, it is hard to directly detect the wetness feature in complex plants. Existing methods also fail to address this challenge effectively. mmLeaf [18], which relies solely on SAR data, lacks accuracy in 3D structures. Hydra [36] partially addresses this by fusion SAR and RGB images to enhance feature capture. Currently, no approach efficiently captures wetness features from SAR imaging in intricate 3D environments.

**Motivation:** The limitations above motivate us to rethink the nature of the results of combining the SAR algorithm and mmWave radar in leaf wetness detection. We observe that RGB images under good lighting conditions have a more explainable feature domain, providing high SNR for leaf wetness detection. We intend to interpret the features and enhance the informativeness of mmWave images by borrowing the perspective of RGB images, thus enhancing the accuracy of mmWave-based leaf wetness detection.

### 3 Proteus Design

We present Proteus an advanced mmWave SAR imaging system for leaf wetness detection shown in Figure 4. We want to introduce the principle of SAR imaging (§3.1), SAR imaging noise reduction (§3.2), Phase Angle enhanced rich texture SAR image (§3.3), Cross-modality Teacher-Student Network Feature Extraction (§3.4), and Depth Fusion (§3.5).

#### 3.1 SAR Imaging

In this section, we present our imaging system based on SAR technology. This system emits signals at regular intervals

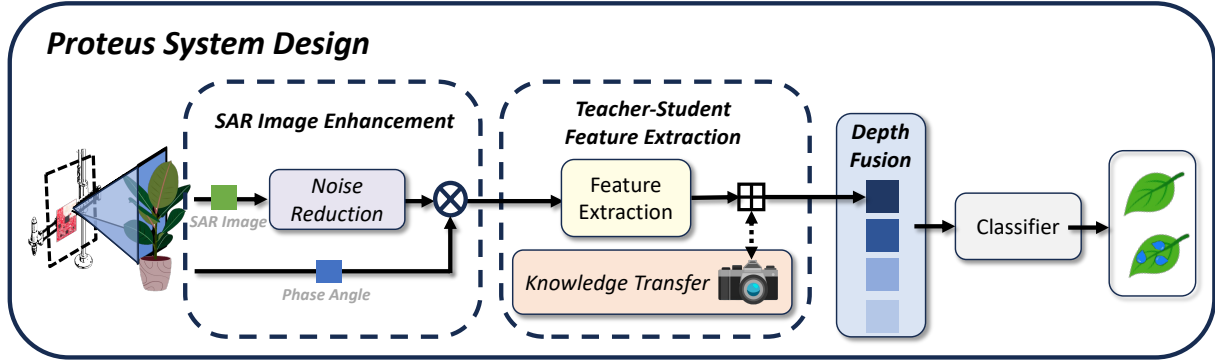


**Figure 4: Proteus Model Overview:** The Proteus model consists of three main components: Noise Reduction, Phase Angle-Enhanced SAR Imaging, and a Teacher-Student Network for Feature Extraction.

to capture images of relatively stationary targets. A key advantage of SAR is its ability to increase the aperture size for higher-resolution images. Combined with FMCW, this approach offers a cost-effective solution for near-field imaging [41, 63, 80, 81]. Our approach is based on the testbed and algorithm produced in [36, 81].

We use the FMCW signal expressed as a linear function of time:

$$m(t) = \cos[2\pi(f_0t + 0.5Kt^2)], \quad (1)$$

where  $f_0$  is the carrier frequency at  $t = 0$ , and  $K = B/T$  is the frequency modulation slope, determined by the sweep bandwidth  $B$  and chirp duration  $T$ .

Upon receiving the backscattered signal, the radar system applies a dechirping process by mixing the received signal with its in-phase  $s_I(t)$  and quadrature  $s_Q(t)$  components, resulting in a complex beat signal:

$$s(t) = s_I(t) - js_Q(t) = \sigma e^{-j2\pi(f_0\tau+K\tau t - 0.5K\tau^2)}, \quad (2)$$

where  $\tau$  represents the round-trip delay, and  $\sigma$  accounts for the target's reflectivity and amplitude decay.

For spatial representation in the wave number domain, the received signal can be simplified as:

$$s(x', y_T, y_R, k) = \iiint p(x, y, z) e^{-jkR_T} e^{-jkR_R} dx dy dz, \quad (3)$$

where  $R_T$  and  $R_R$  are the distances from the transmitter and receiver to the scatter point, respectively, in the scanning system's Cartesian coordinate system.  $p(x, y, z)$  denotes the scattering amplitude at the spatial point  $(x, y, z)$ . It represents the target's reflectivity properties, which determine the strength of the backscattered radar signal received from each location in the scanning area.

The phase compensation is applied to convert the multi-static to monostatic equivalent, represented as:

$$\bar{s}(x', y') = \iint p(x, y) e^{-j2kR} dx dy, \quad (4)$$

where  $R$  represents the distance to the scatter point, allowing for 2D image extraction. Weyl's representation theorem [77] approximates spherical waves as plane waves, enabling the backscatter data to be expressed as:

$$\tilde{S}(k_x, k_y) = P(k_x, k_y) e^{jk_z Z_0}. \quad (5)$$

where  $k_z$  is the wave number in the  $z$ -direction, related to the wavelength and angle of incidence.  $Z_0$  is the reference distance at which the backscatter data is recorded. The inverse Fourier transform of  $\tilde{S}(k_x, k_y)$  provides the reconstructed 2D image:

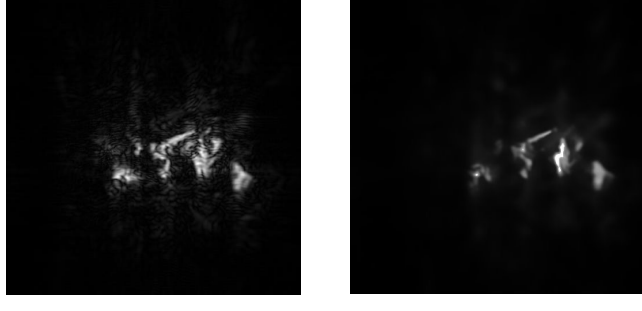
$$p(x, y) = IFT^{(k_x, k_y, k_z)} [e^{-jk_z Z_0} \tilde{S}(k_x, k_y)]. \quad (6)$$

Adjusting the  $x$  range allows for flexibility in balancing the field-of-view and resolution, enabling detailed imaging or faster scans based on specific needs.

### 3.2 Noise Reduction

Noise reduction is a critical step in mmWave SAR imaging due to the inherent presence of speckle noise caused by the coherent nature of the radar signal [56, 62]. Speckle noise arises from the random interference of multiple scatterers within a resolution cell, leading to granular, high-frequency noise in the image [2]. This noise reduces the clarity and quality of the SAR image [47, 74]. Reducing noise is essential to enhancing the SNR, improving image fidelity, and ensuring more accurate feature extraction, particularly for complex tasks like leaf wetness detection. Previous work [1, 8] primarily focuses on visual-based speckle noise reduction. We aim to develop a new denoising technique that enhances model performance in downstream tasks like classification and texture analysis [72].

To address this, we apply a multi-step Computer Vision noise reduction approach that combines several filtering techniques to minimize noise while preserving critical details of the SAR image. The noise reduction process includes



(a) Original SAR Image

(b) Denoised SAR Image

**Figure 5: Comparison of Noise Reduction result.**

Gaussian blur, median blur, and Non-Local Means (NLM) noise reduction. Each step reduces different types of noise while preserving essential features in the SAR image.

The first step involves applying a Gaussian blur to the SAR image. Gaussian blur smooths the image by averaging pixel values based on a Gaussian distribution. It can reduce high-frequency noise while maintaining the overall structure of the image. The Gaussian function for blurring can be expressed as:

$$G(x, y) = \frac{1}{2\pi\sigma^2} e^{-\frac{x^2+y^2}{2\sigma^2}}, \quad (7)$$

where  $(x, y)$  are the pixel coordinates, and  $\sigma$  represents the standard deviation of the Gaussian distribution, controlling the extent of the blurring. In our implementation, we apply a  $3 \times 3$  kernel, which provides a balance between noise reduction and feature preservation:

After Gaussian blurring, we apply a median filter. It effectively removes salt-and-pepper noise while preserving edges, which is crucial for maintaining the sharpness of boundaries in SAR images [40]. In this step, each pixel is replaced by the median value of the surrounding pixels in a  $3 \times 3$  kernel, which helps to remove isolated noise while keeping the image's structural integrity intact.

Finally, we apply Non-Local Means (NLM) noise reduction. NLM works by averaging similar patches across the image, preserving the overall structure and fine details [10, 21]. The NLM noise reduction function is expressed as:

$$NL(v(i)) = \sum_{j \in I} w(i, j)v(j), \quad (8)$$

where  $v(i)$  is the pixel value at location  $i$ ,  $w(i, j)$  is the similarity weight between pixels  $i$  and  $j$ , and  $v(j)$  is the value of pixel  $j$  in the search window. The weights  $w(i, j)$  are calculated as:

$$w(i, j) = \frac{1}{Z(i)} \exp\left(-\frac{|v(i) - v(j)|^2}{h^2}\right), \quad (9)$$

where  $Z(i)$  is a normalization factor and  $h$  is the filtering parameter that controls the degree of smoothing.

Our process effectively reduces speckle noise in SAR images while preserving crucial leaf texture information by combining Gaussian blur, median filter, and NLM noise reduction techniques. The comparison result is shown in Figure 5. This allows for more reliable detection of leaf wetness features, leading to improved system performance and more precise environmental sensing.

### 3.3 Phase Angle Extraction

While SAR images primarily focus on signal intensity, they can miss subtle textural differences. The phase angle provides essential information about the variation in surface texture and roughness variations [4, 9, 32], which can change depending on the leaf wetness. The change occurs due to the dielectric constant and conductivity of wet leaves, which affect the propagation speed of mmWave signals, causing shifts in the phase angle [69]. This integration enables a richer feature with amplitude and phase information for better wetness feature detection.

We begin with the complex beat signal used in Eq. 2 to extract the phase angle from the SAR signal. The in-phase component  $s_I(t)$  and quadrature component  $s_Q(t)$  are used to compute the phase angle  $\phi(t)$ . The phase angle is derived as follows:

$$\phi(t) = \tan^{-1}\left(\frac{s_Q(t)}{s_I(t)}\right). \quad (10)$$

In the wavenumber domain, after compensating for phase shifts, the complex signal  $\tilde{S}(k_x, k_y)$  contains both amplitude and phase information. The phase angle at any spatial point  $(k_x, k_y)$  can be expressed as:

$$\phi(k_x, k_y) = \arg\left(\tilde{S}(k_x, k_y)\right), \quad (11)$$

where  $\arg(\cdot)$  represents the phase of the complex signal. This derivation allows us to extract phase information, which is critical for improving the leaf texture analysis in SAR imaging. The phase angle captures variations in surface properties to alter wave propagation, enhancing the detection of wetness features on leaves.

After deriving the phase angle  $\phi(k_x, k_y)$  from the SAR signal, we enhance the final SAR image by multiplying the phase angle matrix with the SAR amplitude matrix. Multiplying intensity and phase information effectively integrates complementary features while maintaining the inherent relationships between both features. Let  $p(k_x, k_y)$  represent the amplitude of the SAR signal at each point calculated at Eq. 6, and  $\phi(k_x, k_y)$  be the phase angle at the same point calculated at Eq. 11. The final phase-enhanced SAR image  $I(k_x, k_y)$  is obtained by:

$$I(k_x, k_y) = p(k_x, k_y) \cdot \cos(\phi(k_x, k_y)), \quad (12)$$

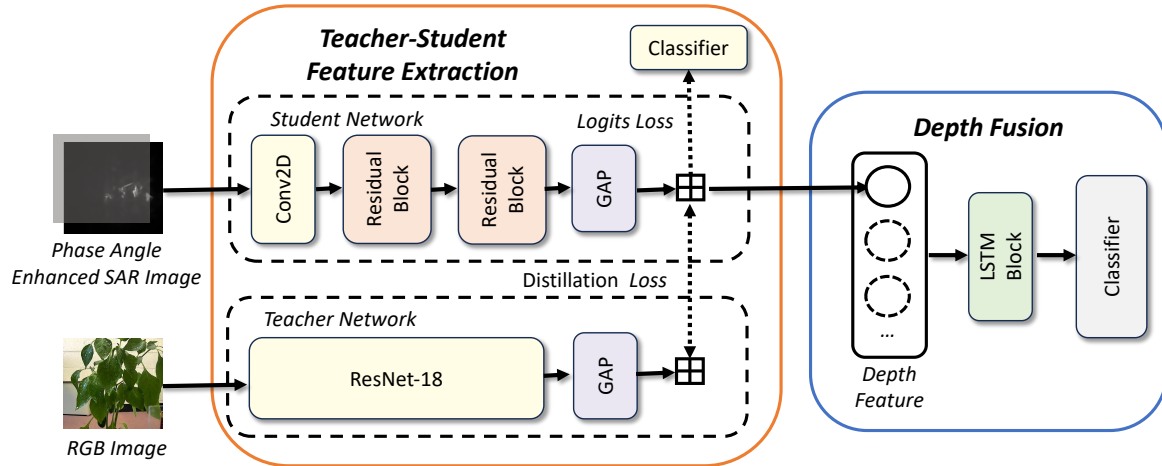


**Figure 6: Teacher-Student network structure with RGB-guided SAR wetness detection and Depth Fusion module.**

where the phase angle adjusts the amplitude values based on the surface characteristics.

This final result incorporates amplitude and phase information, enhancing the SAR image’s ability to detect fine surface wetness features by leveraging the phase angle for improved texture representation.

### 3.4 Cross-Modal Teacher-Student Network

In the previous work, no model could efficiently extract the leaf wetness features from the SAR image. As observed in Section 2.2, SAR imaging with mmWave radar can easily extract the wetness feature from simple leaf structures but struggles with complicated plants. In previous work [36], RGB cameras effectively captured leaf wetness features but struggled in dynamic environments due to lighting dependency. RGB imaging serves as a teacher model to overcome this, guiding the SAR-based model to extract wetness features from mmWave radar more effectively. Our system implements a Teacher-Student Network for feature extraction to enhance the SAR model’s ability to detect leaf wetness, as shown in Figure 6. The teacher model, trained on RGB images, transfers its learned feature representations to the Student model, which processes SAR images. This guidance improves the SAR model’s feature extraction precision and minimizes model size. The student network, designed with only two residual layers, is lightweight and optimized for deployment on edge devices, where computational resources are limited. This reduced complexity enables more efficient and practical implementation in real-time sensing scenarios.

**3.4.1 Model Architecture.** In the teacher model, we use the ResNet-18 network [23] for feature extraction. The exceptional performance of ResNet is excellent in leaf wetness

detection [36]. We design a lightweight architecture for the student model combined with the residual block to enable efficient SAR feature extraction. Each residual block is followed by a dropout layer to prevent over-fitting and improve generalization. Residual layers employ shortcut connections that bypass one layer, enabling the model to learn residual mappings instead of direct mappings [24]. This structure maintains gradient flow across layers, supporting efficient training and helping the student model capture subtle features in SAR images, even when these features are less pronounced.

To further streamline the model, we apply a Global Average Pooling (GAP) layer after the residual layers, which reduces the spatial dimensions and produces a compact feature vector [34]. GAP reduces model complexity, optimizing it for low-power deployment while maintaining accuracy. These outputs are Depth Fusion and classification stages. This depth weight design ensures that the student model can operate effectively on edge devices with limited computational resources and power. The network design is suitable for real-time, in-field agricultural applications.

**3.4.2 Training Processing.** We use a pre-trained teacher model for RGB images to guide the student model’s feature extraction on SAR images. During training, a temporary classifier is attached to the SAR feature extraction layers to serve as a guidance mechanism, helping the student model align with the teacher network’s learned representations. This temporary classifier is removed after training, leaving a streamlined feature extraction process in the final student model.

We use a combined loss function composed of knowledge distillation loss and binary cross-entropy loss to train the student model effectively. Our knowledge distillation loss

model uses cosine similarity to measure the alignment between feature vectors extracted by the Teacher and Student models.

The cosine similarity for knowledge distillation focuses on the directional alignment of feature vectors rather than their magnitude. This is particularly useful in knowledge transfer between different modalities[6, 27]. It encourages the Student model to capture the teacher’s essential patterns and relational structure, regardless of scale differences. After feature extraction, both models pass their outputs through a GAP layer, which reduces each feature map to a 1D vector of consistent size. The Teacher’s feature vector  $f_{\text{teacher}}$  and the Student’s feature vector  $f_{\text{student}}$  is calculated as follows:

$$\begin{aligned}\mathcal{L}_{\text{kd}} &= \frac{f_{\text{teacher}} \cdot f_{\text{student}}}{\|f_{\text{teacher}}\| \|f_{\text{student}}\|} \\ &= \frac{\sum_{i=1}^N f_{\text{teacher}}[i] \cdot f_{\text{student}}[i]}{\sqrt{\sum_{i=1}^N (f_{\text{teacher}}[i])^2} \cdot \sqrt{\sum_{i=1}^N (f_{\text{student}}[i])^2}}.\end{aligned}$$

For the Binary Cross-Entropy loss measures of the classification accuracy of the Student model by comparing its predictions  $y_{\text{pred}}$  to the true labels  $y_{\text{true}}$ . The binary cross-entropy loss  $\mathcal{L}_{\text{bce}}$  is defined as:

$$\mathcal{L}_{\text{bce}} = - \sum (y_{\text{true}} \log(y_{\text{pred}}) + (1 - y_{\text{true}}) \log(1 - y_{\text{pred}})).$$

The total loss function, which combines both the distillation loss and the binary cross-entropy loss, is given by:

$$\text{Total Loss} = \alpha \cdot \mathcal{L}_{\text{bce}} + (1 - \alpha) \cdot (1 - \mathcal{L}_{\text{kd}}),$$

where  $\alpha$  is a weighting factor that balances the importance of classification accuracy and feature alignment. By employing this Teacher-Student architecture, our system capitalizes on the solid feature extraction capability of the RGB-based Teacher model. This enables the SAR-based Student model to enhance its precision in detecting leaf wetness features while remaining lightweight and efficient for edge deployment.

### 3.5 Depth Fusion

The mmWave radar with FMCW chirp captures precise depth information. Depth is the spatial distance from the radar-specific target cross-sections. By gathering depth data across multiple cross-sections, the radar supports accurate 3D reconstruction, providing a comprehensive view of the plant’s internal layout and structure.

A major challenge in plant analysis is the complexity of plant structures, where overlapping or partially obscured leaves hinder visibility. Traditional line-of-sight methods fail to capture hidden details. While 3D models provide a more detailed representation that can improve analysis accuracy, they require effective feature extraction across multiple

depth levels to capture relevant information [26, 38]. We integrate a Long Short-Term Memory (LSTM) network to address this. LSTM networks were initially developed for sequential data in natural language processing. They are adept at identifying patterns across time steps due to their ability to retain long-term dependencies [36, 82]. Compared to Transformer-based models, LSTM is more lightweight while effectively extracting sequential information. In our approach, the LSTM processes sequential cross-sectional data from different depths, learning relationships between features across these layers. Following the LSTM block, a classifier categorizes the leaf wetness status. We train the model using a binary cross-entropy loss specific in Section 3.4.2, which evaluates the classification accuracy against the ground truth labels, ensuring the network’s work’s effectiveness in recognizing wetness within complex plant structures.

## 4 IMPLEMENTATION

### 4.1 System Setup

We develop a prototype of Proteus, shown in Figure 7, incorporating a SAR imaging system with a two-axis mechanical scanner and a mmWave radar for data collection. The scanner, which has a horizontal range of 150mm and a vertical range of 100mm, moves 11.94mm/s to match the target plant’s synthesis aperture size and dimensions. For large-scale farm applications, as referenced in [36], our prototype can be adapted for railway-based sampling of dense plant areas or deployed on drones for efficient field-wide scanning. The synthetic aperture radar needs transmitters and receivers to be horizontally aligned, which we apply with Texas Instruments (TI) IWR1642 [66] shown in Figure 7a. We utilize a DCA 1000EVM [29] to facilitate initial signal collection and processing. We set it to send 500 frames per second, and the two transmitting antennas alternately emit one chirp signal in each frame. Each chirp signal consists of 256 sampling points, and its frequency will increase from  $f_0 = 77\text{GHz}$  to  $f_T = 80.99\text{GHz}$  with the bandwidth  $B = 3.99\text{GHz}$  and frequency slope  $k = 70.295\text{MHz}/\mu\text{s}$ . As shown in Figure 7b, we also include a camera imaging component for training the cross-modal teacher-student model with Azure Kinect [42]. We use the method mentioned in Hydra [36] to calibrate both modalities to maximize the shared features. In both indoor and outdoor experiments shown in Figure 7c and 7d, plants are imaged at 200–500 mm from the mmWave radar during data collection. For each mmWave imaging process, to capture the 3D structure of the plants, we generate multiple images at specific depths from the closest point to its 300 mm behind at a 10 mm depth interval, ensuring thorough coverage.

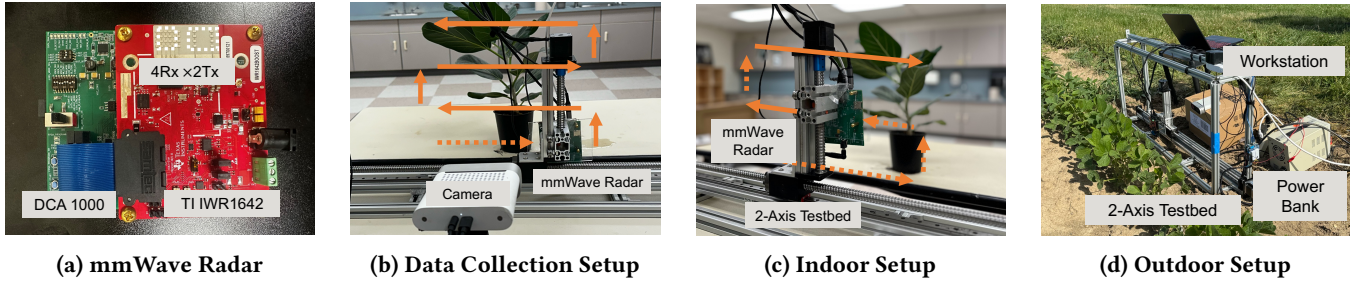


**Figure 7: Proteus comprises a mmWave radar, a two-axis scan testbed, and an RGB camera for training.**



**Figure 8: Moisture Meter for ground truth collection.**

## 4.2 Groundtruth Collection

We adopt a ground truth collection method from Hydra [36], using a commercial moisture meter from General Tools [19] to identify leaf wetness. This device functions by measuring the electrical resistance between two pins, as illustrated in Figure 8. We gently tap the meter’s pins onto the leaf surface to measure the electrical resistance that reflects moisture content. Higher resistance indicates increased moisture levels. Firstly, we record a meter’s reading at room temperature when leaves are completely dry in a well-ventilated indoor environment. We will use the reading as the dryness baseline. For future detection, a reading above this threshold indicates the leaf is wet, and a reading below the threshold indicates the leaf is dry.

## 4.3 Data Collection

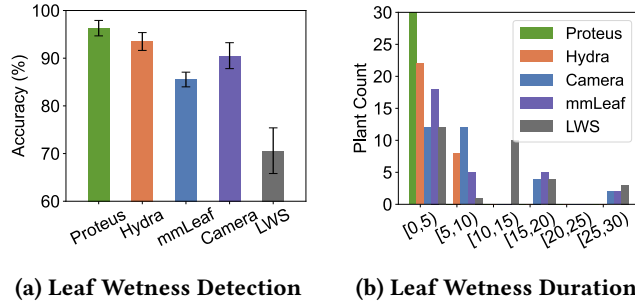
**4.3.1 Leaf Wetness Detection.** Our indoor experiment lasted eight months, during which we collected data from seven diverse plant species with leaf size and orientation variations. Over time, these plants displayed different growth patterns, spacing, and distribution, enhancing the diversity of our dataset. To test Proteus in practical environments, we also conducted in-situ experiments on two fields totaling 3.67 acres, planted with soybeans and corn. These field experiments were conducted under various conditions, including different times of day and weather conditions, such as sunny, windy, and post-rain. For the wind scenario, we

focus mainly on mild wind conditions. Based on [28, 75], leaf wetness leading to disease typically requires a duration of wetness that often lasts several hours. Under strong wind conditions, wetness evaporates quickly, reducing the likelihood of disease development. Other environmental factors, such as temperature and humidity, will have a trivial effect on our system. Humidity-induced signal attenuation is significant over long distances [33], but our focus on near-field imaging, ranging around 200 – 500mm, minimizes this effect. Regarding temperature, the growing season typically experiences temperatures above 28°F / -2°C [45], which falls within the operational range of our radar [66], ensuring reliable performance. We generate a dataset of approximately 724 groups: 536 from indoor environments and 138 from dynamic field conditions. This dataset maximizes the range of wetness levels, allowing Proteus to effectively distinguish wetness features across conditions.

**4.3.2 Leaf Wetness Duration Detection.** To monitor leaf wetness duration with Proteus, we track plants transitioning from saturated wetness to dry states indoors, capturing the drying process at 6 to 12 intervals, each interval being 5 minutes. Our data included 30 groups of measurements across different plants and environmental conditions, highlighting the diversity of wetness features on leaf surfaces.

## 4.4 Baseline

Firstly, we used the commercial LWS PHYTOS 31 [20], the most popular farm application, to monitor leaf wetness. However, we encountered challenges due to the sensor’s metal components, which increased signal reflection and potentially affected data quality for the mmWave system. Since the signal reflection from the LWS will pollute our mmWave images, we place the LWS on a plant of a similar size in the same environment, guaranteeing the same leaf wetness levels. We distributed four LWSs evenly across the plant to capture comprehensive leaf wetness data, providing thorough coverage. We also incorporate methods with mmWave-based systems, including the mmLeaf [18] and Hydra [36] systems and camera-based system [48]. For all the systems,



(a) Leaf Wetness Detection      (b) Leaf Wetness Duration

**Figure 9: Performance of leaf wetness detection.**

we followed the procedures to align our scanning and modeling with established practices, ensuring a comprehensive approach to wetness detection across different systems.

## 4.5 Training Setup

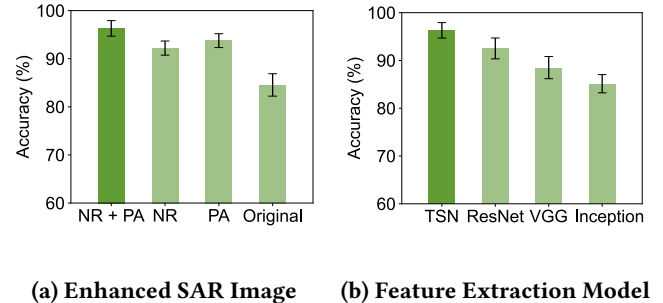
We utilize an NVIDIA RTX 8000 GPU for our training setup to handle both the training and validation processes. The model is trained over 500 epochs with a batch size of 128. The network uses the Adam optimizer with a learning rate of 5e-5. We split the dataset during training, with 80% allocated for training and 20% for validation. Early stopping is also implemented to prevent overfitting, monitoring validation loss with a patience level of 10 epochs. For robust model evaluation, we apply 5-fold cross-validation iterated ten times across diverse datasets.

## 5 EVALUATION

### 5.1 Overall Performance

**5.1.1 Leaf Wetness Detection.** In this part, we evaluate Proteus's ability to distinguish between dry and wet leaves over our leaf wetness detection dataset, which captures indoor and real-field conditions with various lighting and environmental factors. The results are shown in Figure 9a. We can see that Proteus achieves the highest accuracy at  $96.3\% \pm 1.62\%$ , outperforming all baseline models: Hydra achieves the accuracy  $93.5\% \pm 1.87\%$ , mmLeaf for  $85.53\% \pm 1.54\%$ , camera-only for  $90.53\% \pm 2.72\%$ , and LWS for  $70.6\% \pm 4.79\%$ . Compared to the state-of-the-art mmWave-based system mmLeaf, Proteus improves the accuracy by 10.77% and improves the accuracy by 2.8% in compare with Hydra. The result demonstrates Proteus's robust and accurate ability for leaf wetness detection.

**5.1.2 Leaf Wetness Duration.** In this part, we evaluate leaf wetness duration by monitoring the plant's drying process and recording the error of leaf wetness duration over our indoor leaf wetness duration dataset. The results are shown in Figure 9b. Proteus achieve high precision with LWD error consistently within 5 minutes. Compared to the others,



(a) Enhanced SAR Image      (b) Feature Extraction Model

**Figure 10: Enhance SAR with Noise Reduction (NR), Phase Angle (PA), and feature extraction models.**

Hydra records 22 instances within 5 minutes and 8 between 5 and 10 minutes. mmLeaf has 18 within 5 minutes, 5 in the 5–10 minute range, 5 in the 10–15 minute range, and 2 over 15 minutes. The camera method shows 12 instances within 5 minutes, 6 within 5–10 minutes, 4 within 10–15 minutes, and 2 above 15 minutes. LWS has 10 cases within 5 minutes, 12 between 5–10 minutes, 1 within 10–15 minutes, and 7 instances with errors over 15 minutes. The results show that Proteus achieves the highest precision. While the camera accurately detects wetness, as light cannot penetrate leaves to gather comprehensive information. The mmLeaf struggles with feature extraction at low wetness levels. The LWS's inconsistent accuracy relies on synthetic leaves rather than directly sensing actual leaf conditions.

### 5.2 Enhanced SAR Image Performance

In this section, we assess the impact of our SAR image enhancement technique. Our technique includes noise reduction (§ 3.2) and phase angle enhancement (§ 3.3). To assess the effectiveness of these techniques, we conduct an ablation study to compare each enhancement approach with the original SAR images in terms of detection accuracy. Our findings, summarized in Figure 10a, show that traditional SAR images without enhancement have the lowest accuracy  $84.55\% \pm 2.33\%$ . Add phase angle data alone improves accuracy to  $92.21\% \pm 1.47\%$ . Applying noise reduction alone improves accuracy further to  $93.76\% \pm 1.44\%$ . The noise reduction and phase angle combination yield the highest accuracy, reaching  $96.3\% \pm 1.62\%$ . The result shows our technique effectively enhances the SAR image with less inference and rich wetness information.

### 5.3 Cross-Modality Model Performance

We evaluate different feature extraction architectures that perform well in the large classification dataset, including ResNet-18 [23], VGG-16 [60], InceptionV3 [64], and with our Cross-Modal Teacher-Student Network. The results are shown in Figure 10b. Among the direct feature extraction

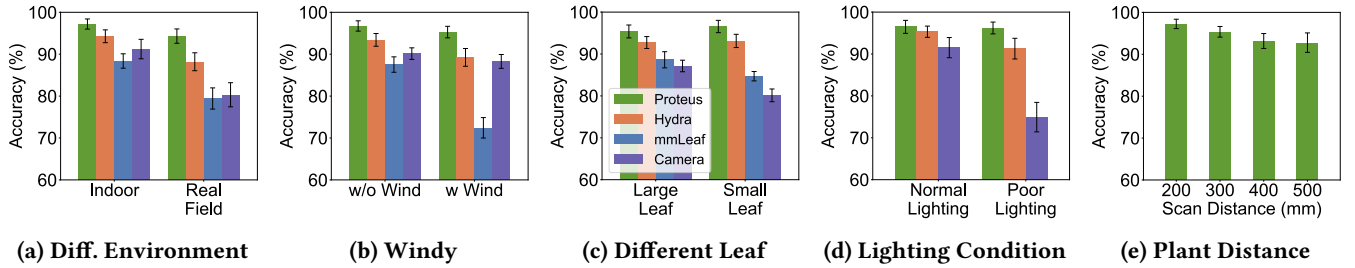


Figure 11: Performance for Proteus application in different scenarios.

models, ResNet-18 achieves the highest accuracy at  $92.52\% \pm 2.18\%$ . VGG16 and InceptionV3 follow, with accuracies of  $88.5\% \pm 2.32\%$  and  $85.13\% \pm 1.91\%$ , respectively. By incorporating our model design, which leverages an RGB-trained Teacher model to guide a SAR-based Student model, we improve accuracy to  $96.3\% \pm 1.62\%$ . This knowledge transfer enables the SAR model to capture deeper wetness features.

#### 5.4 Performance in Dynamic Environments

We evaluate Proteus in both indoor and real farm environments. The focus is on how environmental factors affect wetness detection accuracy and compares to baseline methods, including Hydra, mmLeaf, and the RGB camera. The study includes five scenarios varying in environment, plant type, wind condition, lighting, and distance. The results are summarized in Figure 11.

**5.4.1 Different Environment.** We evaluate in two distinct environments: a controlled indoor lab and a real farm setting, as shown in Figure 11a. In the controlled indoor environment, Proteus achieve the highest precision at  $97.2\% \pm 1.21\%$ . This result underscores the effectiveness of Proteus. In comparison, baseline methods show lower accuracy, with Hydra at  $94.28\% \pm 1.53\%$ , mmLeaf at  $88.38\% \pm 1.72\%$ , and the camera at  $91.23\% \pm 2.32\%$ . In the real farm environment, Proteus demonstrates resilience to dynamic scenarios. It maintains the highest accuracy at  $94.32\% \pm 1.71\%$ . Environmental factors like lighting, wind, and humidity have a more significant effect on baseline methods. Hydra's accuracy slightly drops to  $90.14\% \pm 2.14\%$ . Both mmLeaf and camera perform well in controlled indoor settings, but their accuracy drops in more variable, real-world environments. The mmLeaf drop to  $79.43\% \pm 2.53\%$  and camera drop to  $80.32\% \pm 2.88\%$ .

**5.4.2 Wind Condition.** Wind conditions can significantly impact mmWave systems by changing the intensity of signal reflection. We split the dataset into two categories: one with wind and the other without wind. In the windy dataset, including indoors, a fan simulated a constant wind, and in a real farm setting under moderate natural wind conditions. The

results are shown in Figure 11b. It achieves  $96.74\% \pm 1.23\%$  accuracy in no-wind settings and  $95.28\% \pm 1.38\%$  under windy scenarios. The results show that while mild wind reduces wetness features, our system still accurately detects them. It shows the robustness of our system in a diverse environment. Hydra and camera-based systems also show resilience to wind. Its accuracy drops from  $93.42\% \pm 1.52\%$  in no-wind conditions to  $89.24\% \pm 2.12\%$  under the wind. But the  $4.18\%$  performance drop is much more significant than the  $1.46\%$  degradation of Proteus. The camera system shows a decrease from  $90.14\% \pm 1.38\%$  to  $88.28\% \pm 1.65\%$ . The mmLeaf shows significant degradation, with accuracy falling from  $87.53\% \pm 1.84\%$  to  $72.43\% \pm 2.44\%$  under the wind, indicating it is not reliable to rely on the intensity features solely.

**5.4.3 Plant Type.** We evaluate Proteus on two common plant types: large/sparse and small/dense leaves. Large leaves are prevalent in warm, humid regions to maximize photosynthesis, while smaller leaves are common in cooler, drier areas for better water-use efficiency [49, 78]. Our evaluation is conducted with various plant types indoors, with corn as a large, sparse plant and soybean as a small, dense plant in a real farm setting. As shown in Figure 11c, Proteus achieves high accuracy across both leaf types, reaching  $95.38\% \pm 1.54\%$  on large, sparse leaves and  $96.56\% \pm 1.47\%$  on small, dense leaves. In comparison, Hydra achieves  $92.73\% \pm 1.42\%$  on large leaves and  $93.12\% \pm 1.58\%$  on small leaves; mmLeaf shows more variability with  $88.62\% \pm 1.93\%$  for large leaves and  $84.7\% \pm 2.12\%$  for small leaves; and the camera reaches  $87.14\% \pm 2.38\%$  and  $80.43\% \pm 2.52\%$ , respectively. These results indicate Proteus's superior adaptability and accuracy, particularly in complex plant structures where baseline methods struggle with feature extraction.

**5.4.4 Lighting Condition.** We evaluate the impact of lighting conditions on Proteus. In an indoor environment, we simulate various lighting intensities, while outdoor data is captured at different times, including morning as normal lighting and dawn/night as poor lighting. The results in Figure 11d show that Proteus maintains high precision across lighting conditions, achieving  $96.48\% \pm 1.55\%$  in normal light

**Table 1: Comparison between Proteus and Hydra++ for Inference computational cost and the accuracy**

Metric	Proteus	Hydra++
Extract Feature Time	0.0907 seconds	0.1130 seconds
Extract Feature Mem.	0.69 MB	0.89 MB
Total Time	1.1183s	3.1579s
Total Memory	1.43 MB	2.10 MB
Accuracy	96.3%	97.47%

and  $96.21\% \pm 1.41\%$  in poor light. By comparison, Hydra shows a slight decrease from  $95.32\% \pm 1.34\%$  under normal lighting to  $91.28\% \pm 2.47\%$  in poor lighting since the camera modality stops working. The camera system experiences a more dramatic drop, from  $91.52\% \pm 2.41\%$  to  $74.93\% \pm 3.52\%$ .

**5.4.5 Plant Distance.** The performance of Proteus is further evaluated by measuring its accuracy at varying distances from a target plant in the range of [200 mm, 500 mm]. As shown in Figure 11e, Proteus achieves its highest accuracy of  $96.73\% \pm 1.12\%$  at a 200 mm distance. At 300 mm and 400 mm, accuracy slightly decreases to  $95.32\% \pm 1.27\%$  and  $94.18\% \pm 1.42\%$ , respectively. At 500 mm, accuracy declines to  $92.18\% \pm 1.53\%$ . The increased distance will inevitably reduce mmWave SAR imaging resolution. These results demonstrate that while Proteus remains robust across different distances within 500 mm with high precision.

## 5.5 Performance of Enhanced Hydra

The enhanced SAR imaging approach can be applied across various SAR applications to reduce noise and richer texture information. For example, Hydra [36] fuses mmWave and RGB data for leaf wetness detection. We develop Hydra++, replacing the original SAR images in Hydra with our enhanced approach to denoising and phase angle. In this section, with the leaf wetness detection dataset, we compare Proteus with Hydra++. Table 1 summarizes the key metrics, showing that Hydra++ achieves the highest accuracy at 97.47%, slightly surpassing Proteus at 96.3%. This is because the multi-modal fusion in Hydra++ exploits more information than Proteus with the same quality of mmWave images. Together with the result shown in Figure 9a, Hydra++ outperforms Hydra by 2.97%, verifying the importance of enhancing the mmWave image quality. However, this increased accuracy in Hydra++ comes at a higher computational cost, with an average total process time of 3.1579 seconds and memory usage of 2.10 MB for inference. In contrast, Proteus operates with only 1.1183 seconds of processing time and 1.43 MB of memory usage, making it more efficient. Overall, Proteus and Hydra++ provide alternative solutions for accurate leaf wetness detection.

There is a tradeoff between accuracy and computation efficiency. Proteus has the potential to be deployed on edge, but Hydra++ is better to be deployed on the cloud.

## 6 RELATED WORK

**Leaf Water Content.** Leaf Water Content (LWC) and Leaf Wetness Duration (LWD) are distinct yet complementary indicators of plant disease. LWC refers to the amount of water within the leaf's tissue. Recent advancements in wireless technologies have enabled non-invasive monitoring of LWC, including RFID, backscatter, mmWave, and photonic-crystal resonance [7, 11, 12, 25]. These methods provide real-time data without damaging the plant, making them ideal for continuous monitoring in precision agriculture.

**Cross-Modality Sensing.** Cross-modality sensing combines data from multiple sensors, such as RF, IMU, structural vibrations, RGB, and infrared, to enhance detection and feature extraction across various applications. It has improved gait recognition [79], occupant detection [85], food tracking and quality assessment [58], robotic sensing [73], and imaging with high resolution and robustness [83].

**Artificial Agricultural Internet of Things.** The Internet of Things (IoT) in agriculture combined with artificial intelligence [59] enhances rural connectivity and disease management through precise sensing. For Communication, approaches like LoRa and satellite-based networks improve data reliability over long distances [14, 17, 50–52]. Sensing methods, including RF and VNIR for soil monitoring and reinforcement learning for irrigation control, optimize resource use and support crop health [13, 71].

## 7 CONCLUSION

In this paper, we introduced Proteus, a novel mmWave-based system for accurate leaf wetness detection and Leaf Wetness Duration measurement. Leveraging the sensitivity of mmWave SAR, Proteus effectively captures subtle surface changes on plant leaves. By emphasizing an SAR imaging perspective, Proteus enhances key features and employs a cross-modality model tailored for agricultural applications. Our system significantly reduces speckle noise and enriches SAR images with enhanced texture details. Additionally, we implemented a cross-modality teacher-student network where an RGB-trained teacher model guides the SAR-based student model. Our comprehensive evaluation demonstrates that Proteus achieves up to 96% accuracy across diverse environmental conditions.

## Acknowledgement

We sincerely thank the anonymous reviewers and our shepherd for their valuable feedback. This work was partially supported by NSF CAREER Award 2338976.

## References

- [1] F. Argenti and L. Alparone. 2002. Speckle removal from SAR images in the undecimated wavelet domain. *IEEE Transactions on Geoscience and Remote Sensing* 40, 11 (2002), 2363–2374. <https://doi.org/10.1109/TGRS.2002.805083>
- [2] Fabrizio Argenti, Alessandro Lapini, Tiziano Bianchi, and Luciano Alparone. 2013. A tutorial on speckle reduction in synthetic aperture radar images. *IEEE Geoscience and remote sensing magazine* 1, 3 (2013), 6–35.
- [3] Athanasios Balafoutis, Bert Beck, Spyros Fountas, Jurgen Vangeyte, Tamme Van der Wal, Iria Soto, Manuel Gómez-Barbero, Andrew Barnes, and Vera Eory. 2017. Precision agriculture technologies positively contributing to GHG emissions mitigation, farm productivity and economics. *Sustainability* 9, 8 (2017), 1339.
- [4] Mark P. Blodgett and Daniel Eylon. 2001. The Influence of Texture and Phase Distortion on Ultrasonic Attenuation in Ti-6Al-4V. *Journal of Nondestructive Evaluation* 20, 1 (2001), 1–16. <https://doi.org/10.1023/A:1010611829059>
- [5] Rodrigo Bongiovanni and Jess Lowenberg-Deboer. 2004. Precision Agriculture and Sustainability. *Precision Agriculture* 5, 4 (Aug 2004), 359–387. <https://doi.org/10.1023/B:PRAG.0000040806.39604.aa>
- [6] Elia Bruni, Nam-Khanh Tran, and Marco Baroni. 2014. Multimodal distributional semantics. *Journal of artificial intelligence research* 49 (2014), 1–47.
- [7] Mark Cardamis, Hong Jia, Hao Qian, Wenyao Chen, Yihe Yan, Oula Ghannoum, Aaron Quigley, Chung Tung Chou, and Wen Hu. 2024. Leafeon: Towards Accurate, Robust and Low-cost Leaf Water Content Sensing Using mmWave Radar. *arXiv preprint arXiv:2410.03680* (2024).
- [8] Hyunho Choi and Jechang Jeong. 2019. Speckle noise reduction technique for SAR images using statistical characteristics of speckle noise and discrete wavelet transform. *Remote Sensing* 11, 10 (2019), 1184.
- [9] Magnus Cinthio, Hideyuki Hasegawa, and Hiroshi Kanai. 2011. Initial phantom validation of minute roughness measurement using phase tracking for arterial wall diagnosis non-invasively in vivo. *IEEE Transactions on Ultrasonics, Ferroelectrics, and Frequency Control* 58, 4 (2011), 853–857. <https://doi.org/10.1109/TUFFC.2011.1879>
- [10] Pierick Coupe, Pierre Hellier, Charles Kervrann, and Christian Barillot. 2009. Nonlocal means-based speckle filtering for ultrasound images. *IEEE Transactions on Image Processing* 18, 10 (2009), 2221–2229. <https://doi.org/10.1109/TIP.2009.2024064>
- [11] Spyridon Nektarios Daskalakis, George Goussetis, Stylianos D Assimonis, Manos M Tentzeris, and Apostolos Georgiadis. 2018. A uW backscatter-morse-leaf sensor for low-power agricultural wireless sensor networks. *IEEE Sensors Journal* 18, 19 (2018), 7889–7898.
- [12] Shuvashis Dey, Emran Md Amin, and Nemai Chandra Karmakar. 2020. Paper based chipless RFID leaf wetness detector for plant health monitoring. *IEEE Access* 8 (2020), 191986–191996.
- [13] Xianzhong Ding and Wan Du. 2022. DRLIC: Deep Reinforcement Learning for Irrigation Control. In *2022 21st ACM/IEEE International Conference on Information Processing in Sensor Networks (IPSN)*. 41–53. <https://doi.org/10.1109/IPSN54338.2022.00011>
- [14] Adwait Dongare, Revathy Narayanan, Akshay Gadre, Anh Luong, Arthur Balanuta, Swarun Kumar, Bob Iannucci, and Anthony Rowe. 2018. Charm: Exploiting Geographical Diversity through Coherent Combining in Low-Power Wide-Area Networks. In *2018 17th ACM/IEEE International Conference on Information Processing in Sensor Networks (IPSN)*. 60–71. <https://doi.org/10.1109/IPSN.2018.00013>
- [15] Helen N. Fones, Daniel P. Bebb, Thomas M. Chaloner, William T. Kay, Gero Steinberg, and Sarah J. Gurr. 2020. Threats to global food security from emerging fungal and oomycete crop pathogens. *Nature Food* 1, 6 (Jun 2020), 332–342. <https://doi.org/10.1038/s43016-020-0075-0>
- [16] Spyros Fountas, Katerina Aggelopoulos, and Theofanis A. Gemtos. 2015. *Precision Agriculture*. John Wiley & Sons, Ltd, Chapter 2, 41–65. <https://doi.org/10.1002/9781118937495.ch2> arXiv:<https://onlinelibrary.wiley.com/doi/pdf/10.1002/9781118937495.ch2>
- [17] Akshay Gadre, Zachary Manchester, and Swarun Kumar. 2024. Adapting LoRa Ground Stations for Low-latency Imaging and Inference from LoRa-enabled CubeSats. *ACM Trans. Sen. Netw.* 20, 5, Article 102 (July 2024), 30 pages. <https://doi.org/10.1145/3675170>
- [18] Maolin Gan, Yimeng Liu, Li Liu, Chenshu Wu, Younsuk Dong, Huacheng Zeng, and Zhichao Cao. 2023. Poster: mmLeaf: Versatile Leaf Wetness Detection via mmWave Sensing. In *Proceedings of ACM MobiSys*.
- [19] General Tool. 2024. Moisture Meter. <https://generaltools.com/digital-tools/moisture-humidity-digital-tools/moisture-meters>. Accessed: 2024-10-28.
- [20] METER Group. 2021. *PHYTOS 31 Manual Web*. METER Group. Retrieved Nov 21, 2022 from [http://library.metergroup.com/Manuals/20434\\_PHYTOS31\\_Manual\\_Web.pdf](http://library.metergroup.com/Manuals/20434_PHYTOS31_Manual_Web.pdf)
- [21] Y. Guo, Y. Wang, and T. Hou. 2011. Speckle filtering of ultrasonic images using a modified non local-based algorithm. *Biomedical Signal Processing and Control* 6, 2 (2011), 129–138. <https://doi.org/10.1016/j.bspc.2010.10.004> Special Issue: The Advance of Signal Processing for Bioelectronics.
- [22] Remigio A Guzman-Plazola, R. Michael Davis, and James J Marois. 2003. Effects of relative humidity and high temperature on spore germination and development of tomato powdery mildew (*Leveillula taurica*). *Crop Protection* 22, 10 (2003), 1157–1168. [https://doi.org/10.1016/S0261-2194\(03\)00157-1](https://doi.org/10.1016/S0261-2194(03)00157-1)
- [23] Kaiming He, Xiangyu Zhang, Shaoqing Ren, and Jian Sun. 2016. Deep Residual Learning for Image Recognition. In *IEEE CVPR*.
- [24] Kaiming He, Xiangyu Zhang, Shaoqing Ren, and Jian Sun. 2016. Deep Residual Learning for Image Recognition. In *Proceedings IEEE CVPR*.
- [25] NA Hoog, TE van den Berg, and HS Bindra. 2022. A 60 GHz pulsed coherent radar for online monitoring of the withering condition of leaves. *Sensors and Actuators A: Physical* 343 (2022), 113693.
- [26] Rui Huang, Wanyue Zhang, Abhijit Kundu, Caroline Pantofaru, David A Ross, Thomas Funkhouser, and Alireza Fathi. 2020. An lstm approach to temporal 3d object detection in lidar point clouds. In *Computer Vision–ECCV 2020: 16th European Conference, Glasgow, UK, August 23–28, 2020, Proceedings, Part XVIII 16*. Springer, 266–282.
- [27] Zhenhua Huang, Xin Xu, Juan Ni, Honghao Zhu, and Cheng Wang. 2019. Multimodal Representation Learning for Recommendation in Internet of Things. *IEEE Internet of Things Journal* 6, 6 (2019), 10675–10685. <https://doi.org/10.1109/JIOT.2019.2940709>
- [28] L Huber and TJ Gillespie. 1992. Modeling leaf wetness in relation to plant disease epidemiology. *Annual review of phytopathology* 30, 1 (1992), 553–577.
- [29] Texas Instruments. 2024. DCA1000EVM. <https://www.ti.com/tool/DCA1000EVM>. Accessed: 2024-Oct-28.
- [30] Akash Kumar Kondaparthi, Won Suk Lee, and Natalia A. Peres. 2024. Utilizing High-Resolution Imaging and Artificial Intelligence for Accurate Leaf Wetness Detection for the Strawberry Advisory System (SAS). *Sensors* 24, 15 (2024). <https://doi.org/10.3390/s24154836>
- [31] Milan Koumans, Daan Meulendijks, Haiko Middeljans, Djero Peeters, Jacob C. Douma, and Dook van Mechelen. 2024. Physics-assisted machine learning for THz time-domain spectroscopy: sensing leaf wetness. *Scientific Reports* 14, 1 (25 Mar 2024), 7034. <https://doi.org/10.1038/s41598-024-57161-4>
- [32] Yumeng Liang, Anfu Zhou, Huanhuan Zhang, Xinze Wen, and Huadong Ma. 2021. FG-LiquidID: A Contact-less Fine-grained Liquid Identifier by Pushing the Limits of Millimeter-wave Sensing. *Proceedings of ACM UbiCom* (2021).

- [33] Hans J. Liebe, Kenneth C. Allen, George R. Hand, Robert H. Espeleand, and Edmond J. Violette. 1985. *Millimeter-Wave Propagation in Moist Air: Model Versus Path Data*. Technical Report NTIA Report 85-171. Institute for Telecommunication Sciences, National Telecommunications and Information Administration, Boulder, Colorado. [https://its.ntia.gov/publications/download/85-171\\_ocr.pdf](https://its.ntia.gov/publications/download/85-171_ocr.pdf)
- [34] M Lin. 2013. Network in network. *arXiv preprint arXiv:1312.4400* (2013).
- [35] Yimeng Liu, Maolin Gan, Gen Li, Younsuk Dong, and Zhichao Cao. 2025. Adonis: Neural-enhanced Leaf Wetness Sensing with Efficient mmWave Imaging. In *Proceedings of IEEE INFOCOM*.
- [36] Yimeng Liu, Maolin Gan, Huaili Zeng, Liu Li, Younsuk Dong, and Zhichao Cao. 2024. Hydra: Accurate Multi-Modal Leaf Wetness Sensing with mm-Wave and Camera Fusion. In *Proceedings of ACM MobiCom*.
- [37] C. Lopez-Martinez and X. Fabregas. 2003. Polarimetric SAR speckle noise model. *IEEE Transactions on Geoscience and Remote Sensing* 41, 10 (2003), 2232–2242. <https://doi.org/10.1109/TGRS.2003.815240>
- [38] Na Lu, Yidan Wu, Li Feng, and Jinbo Song. 2018. Deep learning for fall detection: Three-dimensional CNN combined with LSTM on video kinematic data. *IEEE journal of biomedical and health informatics* 23, 1 (2018), 314–323.
- [39] SJ MacKenzie and NA Peres. 2012. Use of leaf wetness and temperature to time fungicide applications to control anthracnose fruit rot of strawberry in Florida. *Plant disease* 96, 4 (2012), 522–528.
- [40] Alenrex Maity, Anshuman Pattanaik, Santwana Sagnika, and Santosh Pani. 2015. A Comparative Study on Approaches to Speckle Noise Reduction in Images. In *2015 International Conference on Computational Intelligence and Networks*. 148–155. <https://doi.org/10.1109/CINE.2015.36>
- [41] Adriano Meta, Peter Hoogeboom, and Leo P Ligthart. 2007. Signal processing for FMCW SAR. *IEEE Transactions on Geoscience and Remote Sensing* 45, 11 (2007), 3519–3532.
- [42] Microsoft. 2024. Azure Kinect DK. <https://www.microsoft.com/en-us/d/azure-kinect-dk/8pp5vxmd9nhq?msockid=0466eb3fd85864550530ff66d94b6503&activetab=pivot:overviewtab>. Accessed: 2024-10-28.
- [43] Concepció Moragrega and Isidre Llorente. 2023. Effects of Leaf Wetness Duration, Temperature, and Host Phenological Stage on Infection of Walnut by Xanthomonas arboricola pv. juglandis. *MDPI Plants* 12, 15 (2023). <https://doi.org/10.3390/plants12152800>
- [44] Concepció Moragrega and Isidre Llorente. 2023. Effects of Leaf Wetness Duration, Temperature, and Host Phenological Stage on Infection of Walnut by Xanthomonas arboricola pv. juglandis. *MDPI Plants* 12, 15 (2023). <https://doi.org/10.3390/plants12152800>
- [45] Natural Resources Conservation Service. 2023. Growing Season Dates and Length. <https://www.nrcs.usda.gov/wps/portal/wcc/home/climateSupport/wetlandsClimateTables/growingSeasonDatesLength> Accessed: 2025-02-06.
- [46] Brian H Nguyen, Gregory S Gilbert, and Marco Rolandi. 2023. A Bio-Mimetic Leaf Wetness Sensor from Replica Molding of Leaves. *Advanced Sensor Research* 2, 6 (2023), 2200033.
- [47] Saurabh Vijay Parhad, Krishna K Warhade, and Sanjay S Shitole. 2024. Speckle noise reduction in sar images using improved filtering and supervised classification. *Multimedia Tools and Applications* 83, 18 (2024), 54615–54636.
- [48] Arth Patel, Won Suk Lee, Natalia A Peres, and Clyde W Fraisse. 2021. Strawberry plant wetness detection using computer vision and deep learning. *Smart Agricultural Technology* 1 (2021), 100013.
- [49] Daniel J. Peppe, Dana L. Royer, Bárbara Cariglino, Sofia Y. Oliver, Sharon Newman, Elias Leight, Grisha Enikolopov, Margo Fernandez-Burgos, Fabian Herrera, Jonathan M. Adams, Edwin Correa, Ellen D. Curran, J. Mark Erickson, Luis Felipe Hinojosa, John W. Hogan-son, Ari Iglesias, Carlos A. Jaramillo, Kirk R. Johnson, Gregory J. Jordan, Nathan J. B. Kraft, Elizabeth C. Lovelock, Christopher H. Lusk, Ulo Niinemets, Josep Penuelas, Gillian Rapson, Scott L. Wing, and Ian J. Wright. 2011. Sensitivity of leaf size and shape to climate: global patterns and paleoclimatic applications. *New Phytologist* 190, 3 (2011), 724–739. <https://doi.org/10.1111/j.1469-8137.2010.03615.x> arXiv:<https://nph.onlinelibrary.wiley.com/doi/pdf/10.1111/j.1469-8137.2010.03615.x>
- [50] Yidong Ren, Amalinda Gamage, Li Liu, Mo Li, Shigang Chen, Younsuk Dong, and Zhichao Cao. 2024. SateRIoT: High-performance Ground-Space Networking for Rural IoT. In *Proceedings of ACM MobiCom*.
- [51] Yidong Ren, Gen Li, Yimeng Liu, Younsuk Dong, and Zhichao Cao. 2025. AeroEcho: Towards Agricultural Low-power Wide-area Backscatter with Aerial Excitation Source. In *Proceedings of IEEE INFOCOM*.
- [52] Yidong Ren, Wei Sun, Jialuo Du, Huaili Zeng, Younsuk Dong, Mi Zhang, Shigang Chen, Yunhao Liu, Tianxing Li, and Zhichao Cao. 2024. Demeter: Reliable Cross-soil LPWAN with Low-cost Signal Polarization Alignment. In *Proceedings of ACM MobiCom*.
- [53] Jean B. Ristaino, Prabhu K. Anderson, Daniel P. Bebber, Kate A. Brauman, Nik J. Cunniffe, Nina V. Fedoroff, Cole Finegold, Karen A. Garrett, Christopher A. Gilligan, Christine M. Jones, Michael D. Martin, Graham K. MacDonald, Patrick Neenan, Andrea Records, David G. Schmale, Louise Tateosian, and Qiang Wei. 2021. The persistent threat of emerging plant disease pandemics to global food security. *Proceedings of the National Academy of Sciences of the United States of America* 118, 23 (Jun 2021), e2022239118. <https://doi.org/10.1073/pnas.2022239118> Erratum in: Proc Natl Acad Sci U S A. 2021 Oct 5;118(40):e2115792118. doi: 10.1073/pnas.2115792118.
- [54] Jean B. Ristaino, Pamela K. Anderson, Daniel P. Bebber, Kate A. Brauman, Nik J. Cunniffe, Nina V. Fedoroff, Cambria Finegold, Karen A. Garrett, Christopher A. Gilligan, Christopher M. Jones, Michael D. Martin, Graham K. MacDonald, Patricia Neenan, Angela Records, David G. Schmale, Laura Tateosian, and Qingshan Wei. 2021. The persistent threat of emerging plant disease pandemics to global food security. *Proceedings of the National Academy of Sciences* 118, 23 (2021), e2022239118. <https://doi.org/10.1073/pnas.2022239118>
- [55] Tracy Rowlandson, Mark Gleason, Paulo Sentelhas, Terry Gillespie, Carla Thomas, and Brian Hornbuckle. 2015. Reconsidering leaf wetness duration determination for plant disease management. *Plant Disease* 99, 3 (2015), 310–319.
- [56] Nupur Saxena and Neha Rathore. 2013. A review on speckle noise filtering techniques for SAR images. *International Journal of Advanced Research in Computer Science and Electronics Engineering (IJARCSEE)* 2, 2 (2013), 243–247.
- [57] Jack Schieffer and Carl Dillon. 2015. The economic and environmental impacts of precision agriculture and interactions with agro-environmental policy. *Precision Agriculture* 16, 1 (Feb 2015), 46–61. <https://doi.org/10.1007/s11119-014-9382-5>
- [58] Amit Sharma, Archan Misra, Vengateswaran Subramaniam, and Youngki Lee. 2019. SmrtFridge: IoT-based, user interaction-driven food item & quantity sensing (*SenSys '19*). Association for Computing Machinery, New York, NY, USA, 245–257. <https://doi.org/10.1145/3356250.3360028>
- [59] Shakhrul Iman Siam, Hyunho Ahn, Li Liu, Samiul Alam, Hui Shen, Zhichao Cao, Ness Shroff, Bhaskar Krishnamachari, Mani Srivastava, and Mi Zhang. 2024. Artificial Intelligence of Things: A Survey. *ACM Trans. Sen. Netw.* (Aug. 2024). <https://doi.org/10.1145/3690639> Just Accepted.
- [60] Karen Simonyan and Andrew Zisserman. 2014. Very Deep Convolutional Networks for Large-Scale Image Recognition. *CoRR* abs/1409.1556 (2014). <https://api.semanticscholar.org/CorpusID:>

14124313

- [61] Brajesh K. Singh, Manuel Delgado-Baquerizo, Eleonora Egidi, Emilio Guirado, Jan E. Leach, Hongwei Liu, and Pankaj Trivedi. 2023. Climate change impacts on plant pathogens, food security and paths forward. *Nature Reviews Microbiology* 21, 10 (Oct 2023), 640–656. <https://doi.org/10.1038/s41579-023-00900-7>
- [62] Prabhishhek Singh and Raj Shree. 2016. Analysis and effects of speckle noise in SAR images. In *2016 2nd International Conference on Advances in Computing, Communication, & Automation (ICACCA)(Fall)*. IEEE, 1–5.
- [63] Andrew G Stove. 1992. Linear FMCW radar techniques. In *Proceedings IET Radar and Signal Processing*.
- [64] Christian Szegedy, Vincent Vanhoucke, Sergey Ioffe, Jonathon Shlens, and Zbigniew Wojna. 2015. Rethinking the Inception Architecture for Computer Vision. [arXiv:1512.00567 \[cs.CV\]](https://arxiv.org/abs/1512.00567)
- [65] Nicolas Tapia-Zapata, Andreas Winkler, and Manuela Zude-Sasse. 2024. Occurrence of Wetness on the Fruit Surface Modeled Using Spatio-Temporal Temperature Data from Sweet Cherry Tree Canopies. *Horticulturae* 10, 7 (2024).
- [66] Texas Instruments. 2024. IWR1642. <https://www.ti.com/product/IWR1642>. Accessed: 2024-Oct-28.
- [67] THE WORLD BANK. 2024. Leaf Wetness Sensor, Vantage Pro2™ and EnviroMonitor. <https://www.davisinstruments.com/products/leaf-wetness-sensor-vantage-pro-and-vantage-pro2>. Accessed: 2024-03-15.
- [68] UC SANTA CRUZ. 2024. Leaf wetness sensor will enable better plant disease forecasting and management. <https://news.ucsc.edu/2023/03/leaf-wetness-sensors.html>. Accessed: 2024-03-15.
- [69] Yozo Utsumi and Toshihisa Kamei. 2004. Dielectric permittivity measurements of liquid crystal in the microwave and millimeter wave ranges. *Molecular Crystals and Liquid Crystals* 409, 1 (2004), 355–370. <https://doi.org/10.1080/15421400490433695> arXiv:<https://doi.org/10.1080/15421400490433695>
- [70] Michiel van Dijk, Timothy Morley, Marie-Laure Rau, and Yashar Saghai. 2021. A meta-analysis of projected global food demand and population at risk of hunger for the period 2010–2050. *Nature Food* 2, 7 (Jul 2021), 494–501. <https://doi.org/10.1038/s43016-021-00322-9> Epub 2021 Jul 21.
- [71] Juxing Wang, Yuda Feng, Gouree Kumbhar, Guangjing Wang, Qiben Yan, Qingxu Jin, Robert C. Ferrier, Jie Xiong, and Tianxing Li. 2024. SoilCares: Towards Low-cost Soil Macronutrients and Moisture Monitoring Using RF-VNIR Sensing. In *Proceedings of ACM MobiSys*.
- [72] Jun Wang, Tong Zheng, Peng Lei, and Xiao Bai. 2018. Ground target classification in noisy SAR images using convolutional neural networks. *IEEE Journal of Selected Topics in Applied Earth Observations and Remote Sensing* 11, 11 (2018), 4180–4192.
- [73] Ruihao Wang, Yimeng Liu, and Rolf Müller. 2022. Detection of passageways in natural foliage using biomimetic sonar. *Bioinspiration & Biomimetics* 17, 5 (2022), 056009.
- [74] Xu Wang, Yanxia Wu, Changting Shi, Ye Yuan, and Xue Zhang. 2024. ANED-Net: Adaptive Noise Estimation and Despeckling Network for SAR Image. *IEEE Journal of Selected Topics in Applied Earth Observations and Remote Sensing* 17 (2024), 4036–4051. <https://doi.org/10.1109/JSTARS.2024.3355220>
- [75] Albert Weiss. 1990. Leaf wetness: measurements and models. *Remote Sensing Reviews* 5, 1 (1990), 215–224.
- [76] Dongmei Wen, Aixin Ren, Tao Ji, Isabel Maria Flores-Parra, Xinting Yang, and Ming Li. 2020. Segmentation of thermal infrared images of cucumber leaves using K-means clustering for estimating leaf wetness duration. *International Journal of Agricultural and Biological Engineering* 13, 3 (2020), 161–167.
- [77] H. Weyl. 1919. Ausbreitung elektromagnetischer Wellen über einem ebenen Leiter. *Annalen der Physik* 365, 21 (1919), 481–500. <https://doi.org/10.1002/andp.19193652104>
- [78] Ian J. Wright, Ning Dong, Vincent Maire, I. Colin Prentice, Mark Westoby, Sandra Diaz, Rachael V. Gallagher, Bonnie F. Jacobs, Robert Kooyman, Elizabeth A. Law, Michelle R. Leishman, Ulo Niinemets, Peter B. Reich, Lawren Sack, Rafael Villar, Han Wang, and Peter Wilf. 2017. Global climatic drivers of leaf size. *Science* 357, 6354 (2017), 917–921. <https://doi.org/10.1126/science.aal4760> arXiv:<https://www.science.org/doi/pdf/10.1126/science.aal4760>
- [79] Huanqi Yang, Mingda Han, Mingda Jia, Zehua Sun, Pengfei Hu, Yu Zhang, Tao Gu, and Weitao Xu. 2024. XGait: Cross-Modal Translation via Deep Generative Sensing for RF-based Gait Recognition (*SenSys '23*). Association for Computing Machinery, New York, NY, USA, 43–55. <https://doi.org/10.1145/3625687.3625792>
- [80] Muhammet Emin Yanik and Murat Torlak. 2019. Near-Field MIMO-SAR Millimeter-Wave Imaging With Sparsely Sampled Aperture Data. *IEEE Access* 7 (2019), 31801–31819. <https://doi.org/10.1109/ACCESS.2019.2902859>
- [81] Muhammet Emin Yanik, Dan Wang, and Murat Torlak. 2020. Development and demonstration of MIMO-SAR mmWave imaging testbeds. *IEEE Access* 8 (2020), 126019–126038.
- [82] Yong Yu, Xiaosheng Si, Changhua Hu, and Jianxun Zhang. 2019. A review of recurrent neural networks: LSTM cells and network architectures. *Neural computation* 31, 7 (2019), 1235–1270.
- [83] Feng Zhang, Chenshu Wu, Beibei Wang, and K. J. Ray Liu. 2021. mm-Eye: Super-Resolution Millimeter Wave Imaging. *IEEE Internet of Things Journal* 8, 8 (2021), 6995–7008. <https://doi.org/10.1109/JIOT.2020.3037836>
- [84] Xiyuan Zhang, Xiaohan Fu, Diyan Teng, Chengyu Dong, Keerthivasan Vijayakumar, Jiayun Zhang, Ranak Roy Chowdhury, Junsheng Han, Dezhong Hong, Rashmi Kulkarni, Jingbo Shang, and Rajesh K. Gupta. 2024. Physics-Informed Data Denoising for Real-Life Sensing Systems. In *Proceedings of the 21st ACM Conference on Embedded Networked Sensor Systems (Istanbul, Turkiye) (SenSys '23)*. Association for Computing Machinery, New York, NY, USA, 83–96. <https://doi.org/10.1145/3625687.3625811>
- [85] Yue Zhang, Zhizhang Hu, Uri Berger, and Shijia Pan. 2023. CMA: Cross-Modal Association Between Wearable and Structural Vibration Signal Segments for Indoor Occupant Sensing. In *Proceedings of the 22nd International Conference on Information Processing in Sensor Networks (San Antonio, TX, USA) (IPSN '23)*. Association for Computing Machinery, New York, NY, USA, 96–109. <https://doi.org/10.1145/3583120.3586960>